JOURNAL OF GEOPHYSICAL RESEARCH: SOLID EARTH, VOL. 118, 4910–4921, doi:10.1002/jgrb.50363, 2013

The coupling between very long period seismic events, volcanic tremor, and degassing rates at Mount Etna volcano

Luciano Zuccarello,[1,2] Michael R. Burton,[3] Gilberto Saccorotti,[3] Christopher J. Bean,[2] and Domenico Patanè[1]

Received 18 February 2013; revised 29 August 2013; accepted 30 August 2013; published 19 September 2013.

[1] From December 2005 to January 2006, an anomalous degassing episode was observed at Mount Etna, well-correlated with an increase in volcanic tremor, and in the almost complete absence of eruptive activity. In the same period, more than 10,000 very long period (VLP) events were detected. Through moment tensor inversion analyses of the VLP pulses, we obtained quantitative estimates of the volumetric variations associated with these events. This allowed a quantitative investigation of the relationship between VLP seismic activity, volcanic tremor, and gas emission rate at Mount Etna. We found a statistically significant positive correlation between SO_2 gas flux and volcanic tremor, suggesting that tremor amplitude can be used as a first-order proxy for the background degassing activity of the volcano. VLP volumetric changes and SO_2 gas flux are correlated only for the last part of our observations, following a slight change in the VLP source depth. We calculate that the gas associated with VLP signal genesis contributed less than 5% of the total gas emission. The existence of a linear correlation between VLP and degassing activities indicates a general relationship between these two processes. The effectiveness of such coupling appears to depend upon the particular location of the VLP source, suggesting that conduit geometry might play a significant role in the VLP-generating process. These results are the first report on Mount Etna of a quantitative relationship between the amounts of gas emissions directly estimated through instrumental flux measurements and the quantities of gas mass inferred in the VLP source inversion.

Citation: Zuccarello, L., M. R. Burton, G. Saccorotti, C. J. Bean, and D. Patanè (2013), The coupling between very long period seismic events, volcanic tremor, and degassing rates at Mount Etna volcano, *J. Geophys. Res. Solid Earth*, *118*, 4910–4921, doi:10.1002/jgrb.50363.

1. Introduction

[2] Mount Etna is the largest stratovolcano in Europe and one of the most active and powerful basaltic volcanoes in the world. Etna is a basaltic intraplate volcano located in eastern Sicily in a complex geodynamic framework, where major regional structural lineaments appear to play a role in controlling dynamic volcanic activity [e.g., *Patanè et al*., 2011]. The processes which create volcanism at Etna are not completely understood. Its position at the junction of several major fault systems may produce a weakening of the crust, promoting magma ascent; slab rollback with associated asthenospheric upwelling and mantle plumes has been also proposed to explain Mount Etna's existence [*De Guidi et al*., 2012, and references therein]. Mount Etna exhibits persistent, voluminous degassing from its summit craters and recurrent summit and flank eruptions [*Aiuppa et al*., 2004; *Andronico et al*., 2005; *Burton et al*., 2005; *Behncke et al*., 2006; *Vergniolle and Gaudemer*, 2011; *Patanè et al*., 2013].

[3] During the last decade, the density of seismic monitoring stations equipped with broadband three-component sensors allowed for assessing long-period (LP) and very long period (VLP) seismicity at Etna has steadily increased. This has permitted a significant improvement in our understanding on the link between seismovolcanic signals and eruptive activity [*Alparone et al*., 2003, 2005; *Patanè et al*., 2008; *Di Grazia et al*., 2006, 2009; *Carbone et al*., 2006, 2008]. VLP events are observed at various volcanoes, and in most cases, they occur synchronously with surface eruptive activity, such as eruptions and gas puffing, e.g., at Stromboli volcano, Italy [*Chouet et al*., 2003, 2008]; Fuego volcano, Guatemala [*Lyons and Waite*, 2011]; Erebus, Antarctica [*Aster et al*., 2008; *Rowe et al*., 1998]; Usu, Japan [*Matsubara and Yomogida*, 2004]; Popocatepetl, Mexico [*Arciniega-Ceballos et al*., 2000; *Chouet et al*., 2005]; and Kilauea [*Chouet et al*., 2010].

[4] Several models have been proposed to explain the source mechanism of VLP events, and all require the resonance and/or

[1]Istituto Nazionale di Geofisica e Vulcanologia, Osservatorio Etneo, Sezione di Catania, Italy.
[2]Seismology Laboratory, Geophysics Group, School of Geological Sciences, University College Dublin, Dublin, Ireland.
[3]Istituto Nazionale di Geofisica e Vulcanologia, Sezione di Pisa, Pisa, Italy.

Corresponding author: L. Zuccarello, Istituto Nazionale di Geofisica e Vulcanologia, Osservatorio Etneo, Sezione di Catania, Piazza Roma 2, 95125 Catania, Italy. (luciano.zuccarello@ct.ingv.it)

2169-9313/13/10.1002/jgrb.50363

transport of fluids and gas in magmatic or hydrothermal systems. For example, *Ohminato* [2006] proposed a source model in which VLP events at Satsuma-Iwojima volcano, Japan, are generated by the sudden vaporization of superheated water. Instead, *Chouet et al*. [2003] suggested a model in which VLP events associated with summit explosions at Stromboli volcano are related to pressure changes caused by the ascent of a gas slug in the summit conduit system. This latter model was reproduced both by analogue laboratory experiments [*James et al*., 2004] and by numerical simulations [*O'Brien and Bean*, 2008].

[5] Direct evidences for a link between VLP signals and volcanic gas emissions were first obtained by *Kazahaya et al*. [2011], at Mount Asama volcano, Japan. By combining high-rate SO_2 flux measurements with seismological data, *Kazahaya et al*. [2011] obtained a proportional relationship between VLP pulse moment and SO_2 emission.

[6] Sometimes, VLP activity is linked to the occurrence of LP events, or with volcanic tremor. This is the case, for example, at Popocatepetl volcano (Mexico), where the analysis of LP and VLP events highlighted a common location for both signals [*Chouet et al*., 2005]. In this case, VLPs were attributed to relatively slow movements of fluids, while sharper pressure transients, associated with an expanding gas pocket, would generate LP signals [*Arciniega-Ceballos et al*., 2008]. On Etna, VLP signals are observed both with and without LP oscillations. For example, *Saccorotti et al*. [2007] found no causal relationship between LP/VLP events and tremor activity.

[7] Therefore, VLP signals could provide information not only on the geometry of the shallow portion of the plumbing system but also on the temporal variations of the physical properties of the magma batches stored therein [e.g., *Chouet*, 2003]. Substantial variations in the frequency, amplitude, and waveform characteristics of these signals are interpreted in terms of pressure changes within the magmatic system and thus constitute a potentially useful tool for forecasting eruptive activity [e.g., *Saccorotti et al*., 2007; *Patané et al*., 2008; *Cannata et al*., 2009; *Chouet et al*., 2010; *Patanè et al*., 2013].

[8] Combining geophysical monitoring of volcanoes with geochemical monitoring of volcanic gas emissions allows multidisciplinary insights into the processes controlling magma ascent and eruption. Etna is also one of the most well-monitored volcanoes in the world in terms of gas emissions, with SO_2 fluxes being measured regularly since the 1970s [*Allard et al*., 1997; *Caltabiano et al*., 2004] using increasingly sophisticated technology [*Burton et al*., 2005; *Mori and Burton*, 2006; *Salerno et al*., 2009a, 2009b]. SO_2 flux is a key parameter in understanding the dynamics of a volcanic system because both its absolute magnitude and variability allow constraints to be placed on magmatic processes (see review by *Oppenheimer et al*. [2011]). The absolute value of gas flux is directly related to the magma supply rate to the upper 1–2 km of the magmatic plumbing system, where volatile-rich magmatic systems such as Etna permit open-system degassing [*Burton et al*., 2007]. The volume of magma degassed can be quantified by comparison with the concentration of S originally dissolved in the melt [e.g., *Allard et al*., 1997], which allows direct comparison with geophysical observations. Such measurements can be also combined with measurements of H_2O, CO_2, SO_2, HCl, and HF obtained with open-path infrared spectrometry to yielded direct insight into the magma dynamics within the plumbing system [*La Spina et al*., 2010].

[9] Time variations of geochemical parameters and volcanic tremor have important implications in monitoring volcanic activity and understanding magma dynamics. *Nadeau et al*. [2011] conducted a multiparameter experiment at Fuego volcano (Guatemala) in order to study activity and relationships between degassing and seismic tremor. The authors identified the presence of linked source processes for tremor and degassing, developing a model for small, ash-rich explosions that occurred from isolated vents. Recently, combined seismic (volcanic tremor) and geochemical (SO_2 flux, CO_2 flux, and CO_2/SO_2 ratio) measurements have been studied to understand the volcanic activity, as well as to investigate magma movement in both deep and shallow portions of the plumbing system of Etna volcano [*Aiuppa et al*., 2010; *Patanè et al*., 2013].

[10] Due to the key role of gas flow in producing VLP events, it is natural to ask the question: Is there a direct link between the degassing signature on Mount Etna and the VLP events? Following the aforementioned source models of VLP seismicity, in this paper, we present a quantitative investigation of the relationships between seismic and SO_2 flux data collected at Etna volcano, focusing our analysis on the comparison between very long period (VLP) signals, tremor (TR) seismicity, and degassing activity. Our data span the October 2005 to January 2006 time interval. Seismic recordings from Etna's broadband network are examined together with SO_2 fluxes obtained from both traditional traverses and the automatic Flux Automatic Measurement (FLAME) network of scanning ultraviolet (UV) spectrometers [*Burton et al*., 2005; *Salerno et al*., 2009a].

[11] Quantitative estimates of the volumetric variations associated with VLP events are derived from moment tensor inversion via full-waveform modeling [*Lokmer et al*., 2007; *De Barros et al*., 2011]. Assuming that the VLP source mechanism is related to the transit and decompression of a large gas slug at a conduit's geometrical asperity, and using a lithostatic pressure gradient, we are thus able to constrain the amount of volatiles implied in the VLP-generating process. Furthermore, we use quiescent degassing compositions [*La Spina et al*., 2010] to determine the total volume of gas released in the investigated period, which permits a direct comparison with the volume of gas estimated through the analysis of VLP seismicity.

2. Data

[12] Continuous seismic activity monitoring of Mount Etna is performed by a permanent seismic network which, by the time of our analysis, included 13 broadband stations equipped with Nanometrics Trillium (40 s) three-component seismometers (see Figure 1 for their location). Data are acquired and recorded locally at 100 samples/s/channel through Nanometrics Trident Digital Systems (24 bits) and then transmitted via satellite or radio to the data acquisition center of the Istituto Nazionale di Geofisica e Vulcanologia, Catania.

[13] Gas fluxes are recorded using a permanent, automatic network of ultraviolet (UV) scanners, called FLAME (Flux Automatic Measurements), which was installed in early 2005 [*Burton et al*., 2005; *Salerno et al*., 2009a]. During the period of interest (2005–2006), the FLAME network consisted of five UV scanners installed in the southern and eastern flanks

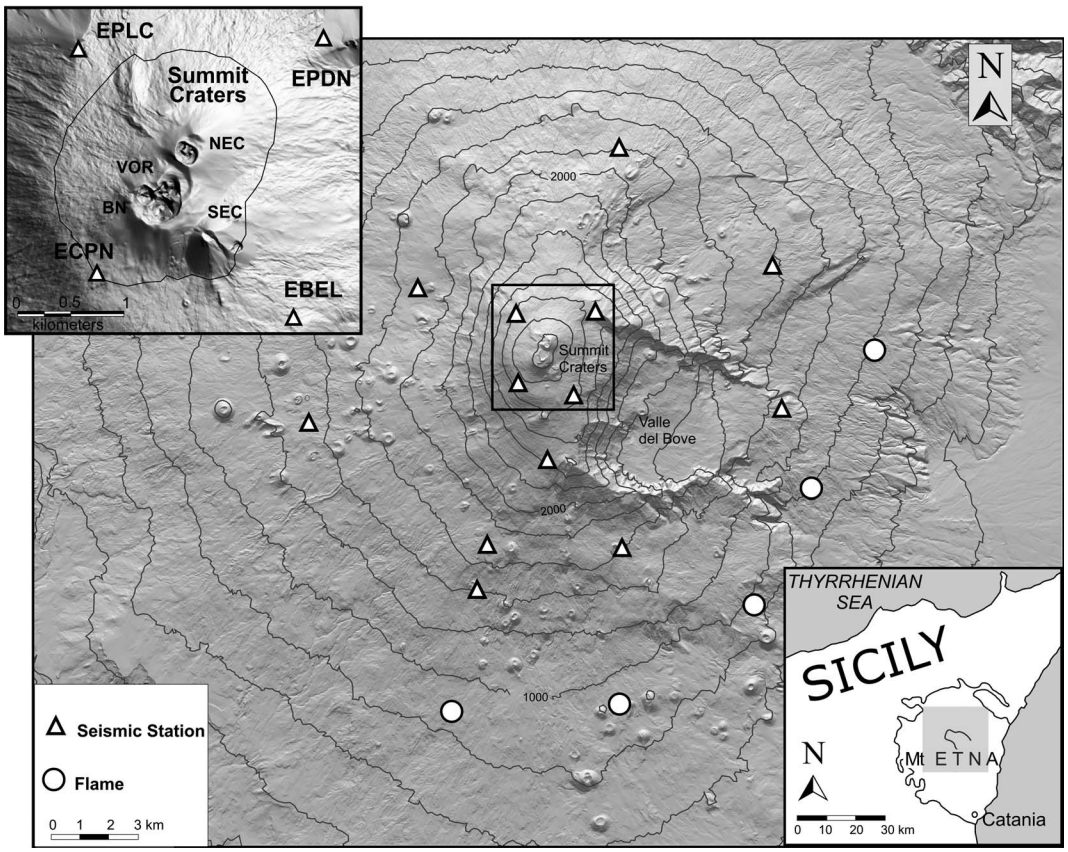

Figure 1. Schematic map showing the position of the digital broadband stations and the five UV scanner stations used in the present study. The inset at the bottom right shows the location of Etna volcano with respect to Sicily; the one at the top left shows the position of the four broadband stations (ECPN, EBEL, EPDN, and EPLC) close to the Summit Craters (NEC = Northeast Crater, VOR = Voragine, BN = Bocca Nuova, SEC = Southeast Crater).

of the volcano (Figure 1). These stations are equipped with an Ocean Optics (www.oceanoptics.com) S2000 spectrometers (2048 pixel detector), which view the sky through a motor-driven scan head which rotates with an angular resolution of 0.06°. Each scan takes approximately 3–5 min to complete, depending on the intensity of skylight. The spectrometer is controlled by an onboard microcontroller, collecting data daily for almost 9 h depending on the season and acquiring a complete scan (105 spectra, including a dark spectrum) in ~6 min [*Salerno et al*., 2009a]. The acquired data are transmitted via a GSM modem to the observatory in Catania, where SO_2 flux data are produced in real time through integration with forecast winds [*Salerno et al*., 2009a]. These continuous data streams are complemented by more traditional, but less frequent, vehicle-driven traverse measurements which were conducted 2–3 times per week [*Salerno et al*., 2009b] during the period of interest. The results presented here represent the fusion of daily average measurements from both SO_2 flux monitoring methods.

2.1. Volcanic Activity and Observations From December 2005 to January 2006

[14] Beginning in early November 2005, ground deformation data collected by the GPS network installed in the summit area suggested pressurization of the upper plumbing system (M. Mattia, personal communication). This inflation was followed by a gradual increase in both the amplitude of volcanic tremor (Figure 2a) and SO_2 flux; this latter reached values larger than 18,000 t/d, which would not be unusual for an eruption (Figure 2b); however, no eruptive activity was observed.

[15] On 16 December 2005, at 13:25 UT, two explosion quakes (Figure 2a) were recorded. Poor weather conditions inhibited the direct observation of any surface activity that may have accompanied these seismic signals. A few hours after these explosions, the amplitude of volcanic tremor increased abruptly, and SO_2 fluxes showed a dramatic increase, reaching more than 18,000 t/d on the following days.

[16] On the morning of 22 December, ash was observed being emitted from the BN (Figure 1) for a few hours. Preliminary study of the erupted material indicated a high amount of juvenile components, consistent with a fresh magmatic input into the shallow plumbing system. Seismic tremor and volcanic degassing remained at high levels, comparable to the 2004–2005 eruption [*Burton et al*., 2005; *Di Grazia et al*., 2006], until an energetic explosion quake occurred on 12 January, at 13:05 UT, shortly before a new ash emission. Despite cloudy weather, the images from Etna's video surveillance system suggested that the ash was emitted from the BN (Figure 1). In this case, the analysis carried out on the ash showed a low level of juvenile components, suggesting that it was produced by a withdrawal of magma

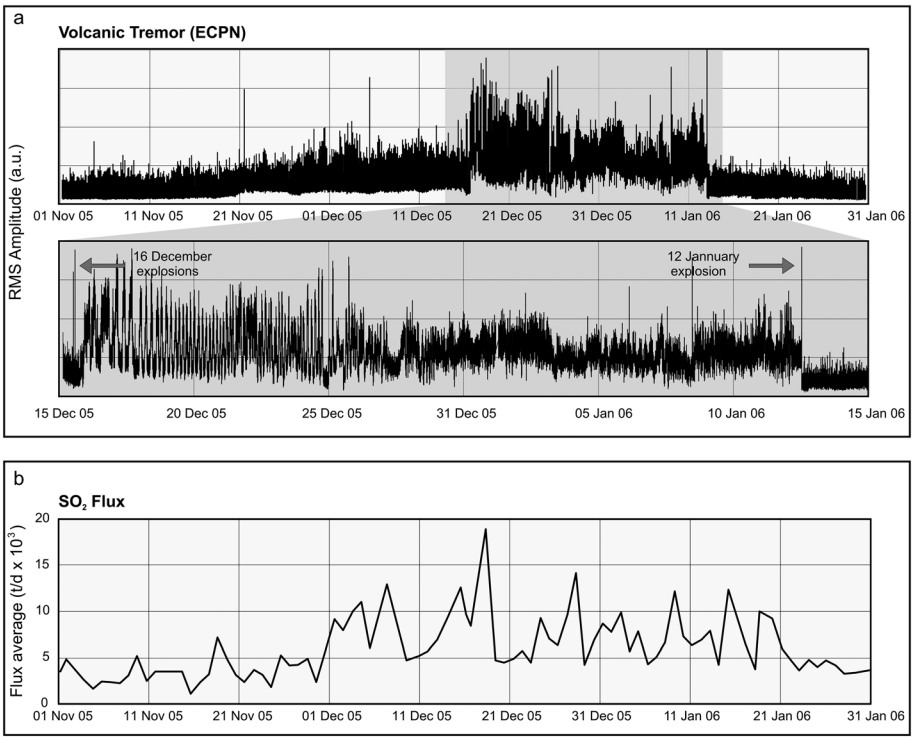

Figure 2. (a) RMS tremor amplitude from the ECPN station, during the 1 November 2005 to 31 January 2006 time interval. (bottom) The marked increase in the amplitude of the volcanic tremor observed at all seismic stations during 15 December 2005 to 12 January 2006. Both the start and the end of this period were marked by energetic explosions from the summit craters zone. (b) SO_2 fluxes recorded by both the traditional traverses and the UV-FLAME network.

from the shallow plumbing system. Resumption of summit eruptive activity occurred 6 months later on 14 July 2006 at the SEC, which was the site of a 10 day long Strombolian-effusive eruption [*Neri et al*., 2006]. After the 12 January 2006 explosion, the volcanic tremor returned to the background level exhibited before November 2005 (Figure 2a).

[17] The most striking feature of the tremor during the period of high amplitude is given by the occurrence of cycles with a period of 2–3 h (Figure 2a) [see also *Carbone et al*., 2008]. The spectral features of the tremor, with multiple peaks spanning the 0.5–5 Hz frequency band, do not appear to change throughout the entire anomalous period and are similar to those observed during the previous months [*Carbone et al*., 2008]. These latter authors found a tight anticorrelation between the signal from the summit gravity station EBEL (Figure 1) and the RMS of the volcanic tremor. This correlation faded away just before the end of the high-tremor period. *Carbone et al*. [2008] inferred a common gravity/tremor source volume located in a region 1 km S-SE of the summit craters at depths of about 2 km beneath the surface. The authors explained this anticorrelation in terms of the arrival of fresh magma and the consequent gas separation, able to contemporaneously trigger tremor activity and to decrease the local value of the gravity acceleration. Superimposed on volcanic tremor, we recorded transient seismic signals with characteristic frequencies spanning the 0.05–0.2 Hz frequency band, which are the object of this study (Figure 3).

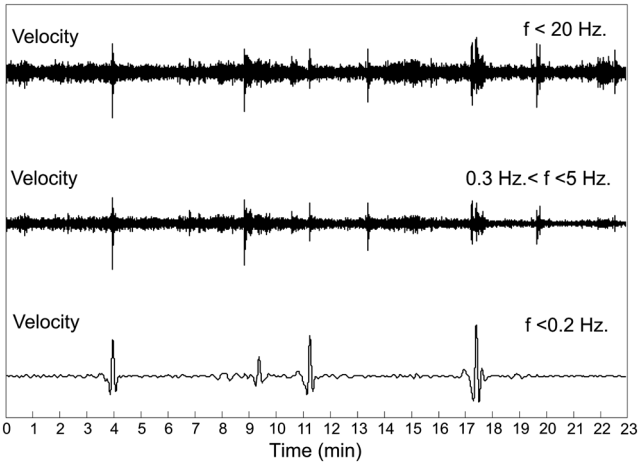

Figure 3. An example of broadband seismic recording at station ECPN (Figure 1) on 21 November. The broadband signal from the vertical component of ground velocity is filtered over different frequency bands to produce three records for the same 23 min time interval. The top trace shows the typical broadband signal ($f < 20$ Hz). The second trace shows the signal after band-pass filtering (0.3 Hz $< f <$ 5 Hz). The result shows a series of events superimposed on a background of tremor. The third trace shows the signal when a low-pass filter is applied ($f < 0.2$ Hz); very long period (VLP) pulses with a dominant period of about 20 s are observed in this record.

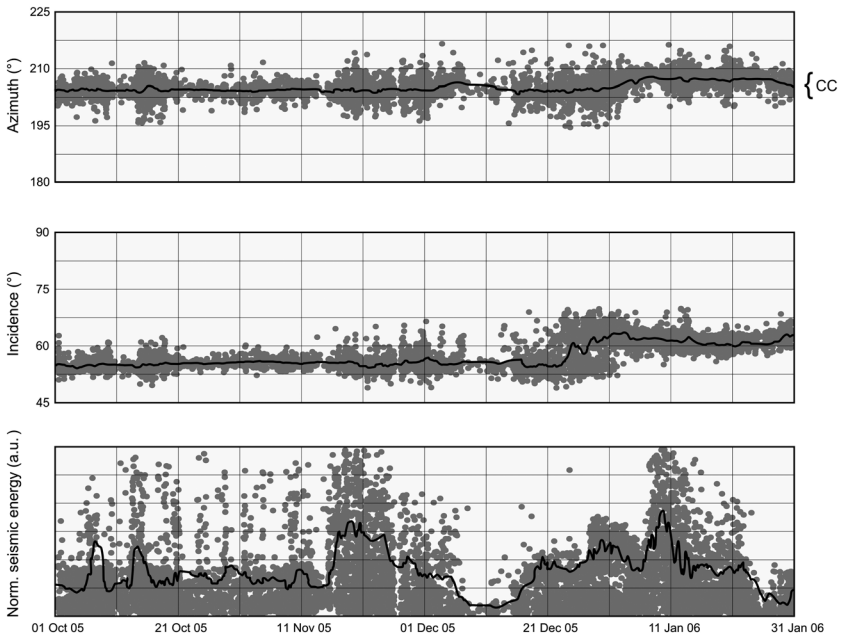

Figure 4. Temporal evolution of the polarization parameters obtained by analyzing the VLP events recorded at the ECPN station. From top to bottom, plots represent distributions of azimuth, incidence angle, and normalized seismic energy derived from the principal axes of the polarization ellipsoid, for which the rectilinearity coefficient is greater than 0.8. The covariance matrix of the three components of ground displacement is calculated over successive, 40 s long windows sliding along the signal with 50% of overlap. The black lines indicate the moving averages on 100 samples. The right bracket on the azimuth distribution indicates the Central Crater position.

3. VLP Signals: Detection and Source Location

3.1. Event Detection

[18] We created a VLP catalog performing the polarization analysis on seismic data recorded at the ECPN station between October 2005 and January 2006. Using the covariance matrix method of *Kanasewich* [1981], we analyzed the particle motion over 40 s long time windows sliding with a 20 s increment along the three-component displacement seismograms, bandpass filtered over the 0.01–0.2 Hz frequency band. Results from the covariance analysis consist of the time series of polarization azimuth and incidence angles, the three-component signal envelope (i.e., the trace of the covariance matrix), and the rectilinearity coefficient [*Kanasewich*, 1981].

[19] From these time series, event discrimination was performed by selecting those peaks in the three-component envelopes for which the coefficient of rectilinearity is larger than 0.8, and the polarization azimuth is oriented radially to the summit craters (i.e., back azimuths between 10°N and 40°N).

[20] In this manner, we were able to detect more than 10,000 VLP transients spanning the October 2005 to January 2006 time interval. After the detection procedure, data were organized in a digital archive containing 200 s long recordings, starting 100 s before the maximum peak-to-peak amplitude.

[21] Variations of polarization ellipsoids with time analyzed at the ECPN station (Figure 1) between October 2005 and January 2006 are shown in Figure 4. The most evident features are as follows: For the first 80 days of measurement (until 20 December 2005), both incidence and azimuth angles are clustered within narrow angular intervals centered at 52°N–57°N and 200°N–210°N, respectively, indicating the action of a single source located some 800–1000 m beneath the summit craters.After 20 December, incidence angles begin to cluster around larger values, indicating the activation of a second, shallower source which rapidly substitutes the previous one. For the retrieved source epicenter (see below), the ~7° change of the incidence angles implies that the second source is about 200 m shallower than the first one. Changes in incidence angles are accompanied by a slight variation of azimuth angles which, however, appears to be barely significant once accounting for the overall fluctuation of the measurements. Several remarkable changes in the release of seismic energy derived from the principal axes of the polarization ellipsoid, the most important of which is the increase occurring between 16 and 21 November, soon followed by a rapid decrease until the occurrence of the two explosions on 16 December 2005. Between the end of December 2005 and the first days of January 2006, a marked new increase in seismic energy release was observed.

[22] Figure 5 illustrates the daily number of VLP detections. The statistical distribution of VLP peak-to-peak displacement amplitudes as measured at the *N* component of station ECPN indicates a mean value around 15 μm (Figure 5b).

3.2. Source Location

[23] The emergent aspect of the VLP waveforms precludes the use of conventional approaches based on traveltime inversion to locate the source. The study of volcanic seismicity requires other approaches, such as location methods based on waveform similarity or particle motions of multichannel

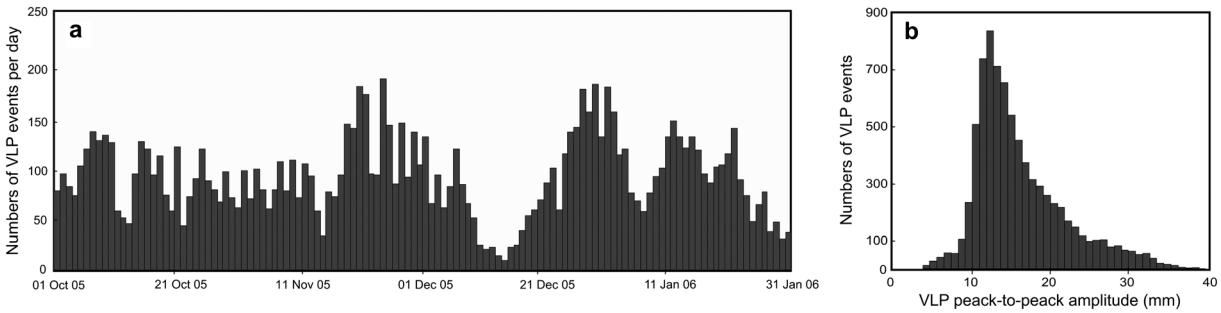

Figure 5. (a) Time distribution of the daily number of VLP events identified during the period under study. The minimum lies in correspondence of the 16 December explosion. (b) Maximum peak-to-peak amplitude (*N* component of displacement) distribution for the about 10,000 VLP pulses detected through the polarization analysis.

data [*Kawakatsu et al.*, 2000; *Marchetti and Ripepe*, 2005; *Cannata et al.*, 2009]. For this reason, we retrieve source locations using two different but complementary techniques: (1) semblance-based grid search method and (2) back projection of the polarization vectors estimated at the summit stations.

[24] We selected a VLP pulse in our catalog, hereafter called the master event, that (i) has the best signal-to-noise ratio and (ii) has been recorded by all the stations located on the top of the volcano (ECPN, EBEL, EPLC, and EPDN; Figure 1). With a maximum peak-to-peak displacement amplitude (*N* component) at ECPN of about 35 μm, this event is among the strongest signals recorded during the period under investigation. To locate this event, we applied the semblance method [*Neidell and Taner*, 1971] to 40 s long windows of signal encompassing the largest amplitude.

[25] Assuming an homogeneous medium with a *P* wave velocity of 1.8 km/s [*De Barros et al.*, 2009], we determined the best location for a single-point source, conducting a grid search over a grid extending 5 × 5 × 2 km, with a node spacing of 50 m, and origin located at ($x = 497$km, $y = 4176$ km, $z = 1.0$ above sea level, in universal transverse Mercator World Geodetic System 1984 coordinates.

[26] The source location obtained with this technique was then checked against the particle motion analysis performed at the stations closest to the crater area to confirm the accuracy of the solution. The source location based on polarization is performed through a search over the same grid described above. For each grid node (source position), we compare the polarization vectors inferred from particle motion with those expected for an isotropic source. Eventually, we select the solutions allowing minimum misfit. We assume an infinite, homogeneous, and isotropic medium; therefore, the expected polarization vectors are derived directly from the straight line joining any given source-station pair.

[27] Under the assumption that errors on the estimates of polarization angles are normally distributed, the likelihood *P* for the source to be located at ($\mathbf{x_0}$) is given by

$$P(\mathbf{x_0}) = \frac{1}{\sqrt{2\pi}\sigma} * \exp^{-\sum_{i=1}^{N}\left(\frac{(\mathbf{xm}-\mathbf{xp})^2}{2\sigma^2}\right)} \quad (1)$$

where [**xm**, **xp**] are unit vectors pointing along the directions of the measured and predicted particle motions, respectively, and σ^2 is the data variance.

[28] This likelihood function is weighted by the spatial distribution of the semblance coefficient, thus obtaining a joint pseudoprobability density function whose maximum indicates the most likely source location (Figure 6).

[29] For locating the rest of the events, we limit our analysis to the back projection of the particle motion vectors obtained at station ECPN onto an EW vertical plane passing through the location obtained from the joint semblance–particle motion inversion of the master event. Results are shown in Figure 7. All the hypocenters are tightly clustered in a small volume whose barycenter lies beneath the summit craters, at an

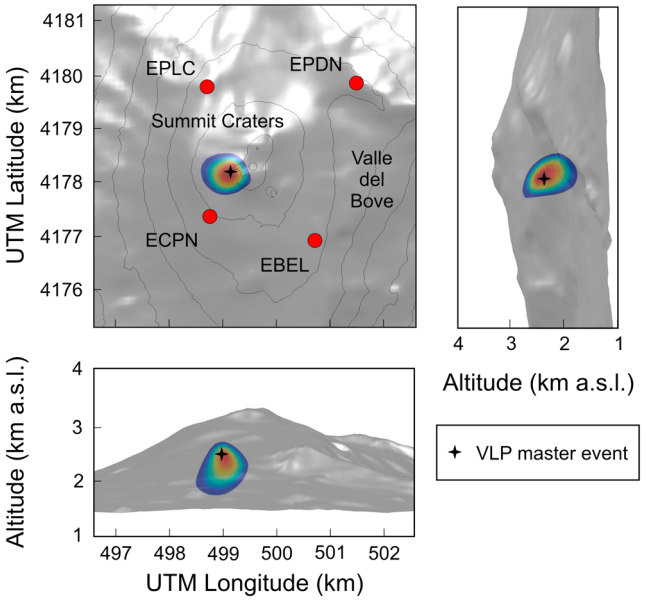

Figure 6. Maximum-likelihood hypocenter locations in (top) map view, (bottom) longitude, and (right) latitude sections. The colored regions border the 70% confidence levels for the probability hypocenter location, obtained by integrating the function [see equation 1] derived from the misfit between the theoretical and measured particle motion vectors for the four summit stations (red dots on the map), weighted by the semblance coefficient. The black star marks the location obtained from the master event by using the semblance method.

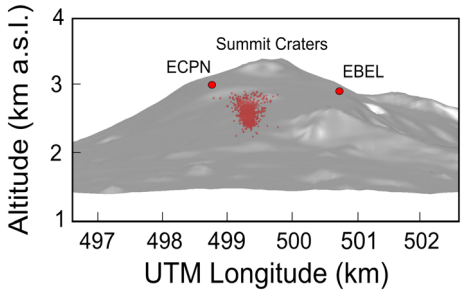

Figure 7. Vertical cross section of Mount Etna with location of the about 10,000 VLP events detected during the 1 October 2005 to 31 January 2006 time interval. The red dots denote the locations obtained by back-projecting particle motion vectors on an E-W vertical plane passing through the location of the VLP master event displayed in Figure 6.

average depth of ≈800–1000 m beneath the surface, about 1000 m N-NE of the ECPN station (Figure 7), in good agreement with the previous results obtained by *Saccorotti et al*. [2007].

[30] In this procedure, we neglected the particle motion distortion as a consequence of the free-surface interaction [*Neuberg and Pointer*, 2000]. From a separate analysis of synthetic seismograms calculated for a homogeneous medium bounded by the realistic 3-D topography of Etna, we noted, however, that such effects are relatively small, e.g., on the order of a few degrees (about 2°), thus implying a maximum error on source depth on the order of 30–50 m.

4. Inferred VLP Volumetric Changes

[31] VLP events are thought to represent the elastic response of the rocks embedding the volcano's plumbing system to transient volumetric changes related to mass transport phenomena, such as the transit and decompression of large gas slugs [e.g., *Chouet*, 2003]. Under this hypothesis, estimates of the volume change at the VLPs should be a constraint on the amount of gas involved in their genesis and therefore allows a comparison with the overall degassing rate.

[32] In a separate study, we are currently analyzing the VLP source mechanism via full-waveform inversion of the seismic moment tensor. Although this companion study has not yet reached a definitive conclusion for which concerns the source mechanism, our preliminary results indicate that a crack-shaped body is the most likely candidate for describing the VLP source.

[33] Using the master event described above, we found that a maximum seismic displacement (*N* component) of about 35 μm at the ECPN station corresponds to an isotropic moment M_i of about 2.8×10^{12} N m. These results are significantly different from those derived by *Saccorotti et al*. [2007], who, for a ground displacement at ECPN of 10 μm, inferred an isotropic moment of 4×10^{12} N m. The origin of such discrepancy resides in two factors: (a) The Green's functions used by *Saccorotti et al*. [2007] were obtained using the analytical solution for an infinite, homogeneous medium, implying an overestimate of the seismic moment of about a factor of 2; and (b) the source-to-receiver distances used by *Saccorotti et al*. [2007] were larger than those adopted here, again implying an overestimate of the source moment.

[34] For the assumed crack-like geometry, the relationship between the isotropic moment and the volume change ΔV is [*Muller*, 2001]

$$M_i = \Delta V(\lambda + 2/3\mu) \tag{2}$$

where λ and μ are Lame's elastic parameters. Assuming $\lambda = 2\mu$ and $\mu = 5.5$ GPa, we obtain a volumetric change ΔV of about 190 m^3 , which is on the same order of magnitude as that obtained at Stromboli volcano by *Choute et al*. [2003].

[35] For fixed source location, source mechanism, and recording site, the ground displacement scales linearly with the isotropic moment. We thus used moment tensor results from a set of 10 additional events of different amplitudes and calculated a linear regression in the form $\Delta V = au + b$, relating volume change at the source to peak ground displacement *u* at station ECPN (Figure 8).

[36] In our fitting procedure, data uncertainties are derived assuming a ground displacement error of 3 μm, which corresponds to the detection threshold of our catalog (Figure 5b). The maximum-likelihood estimate of the fitting parameters yields $a = (6.0 \pm 0.5) \times 10^6$ m^2, and $b = -53 \pm 13$ m^3 ; as a consequence, uncertainties on volume change estimates are on the order of 20–30 m^3. Using displacement seismograms at ECPN, we calculated the maximum peak-to-peak amplitude for each VLP event of our catalog and summed up these values on a daily basis, in order to obtain a time series of cumulative VLP displacement sampled at intervals of 1 day. Then, from the linear relationship described above, we derived the daily cumulative VLP volume changes. This time series is shown in Figure 9, together with the daily SO_2 flux and average tremor amplitude.

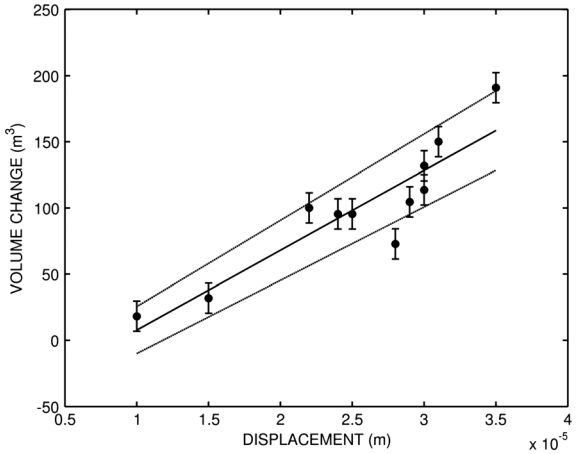

Figure 8. Linear regression between volumetric changes derived from the isotropic component of the moment tensor [see equation 2] and the maximum peak-to-peak displacement amplitude at the *N* component of station ECPN. Error bars on volume change estimates have been derived assuming an uncertainty of 3 μm on the ground displacement data. Dashed lines are the 95% (±2σ) confidence bounds on the best fitting line.

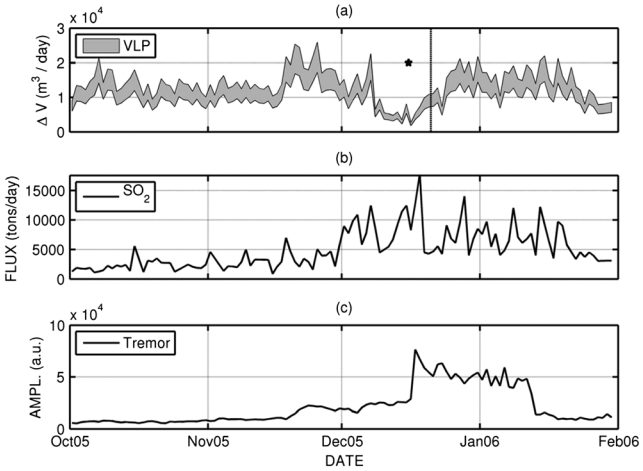

Figure 9. (a) Daily VLP cumulative volume changes. (b) SO_2 gas flux. (c) RMS tremor amplitude. The daily VLP volume changes calculation has been obtained using the linear regression procedure shown in Figure 8. The SO_2 gas flux time series is related to the total degassing rate recorded from the summit craters. The black star indicates the 16 December energetic explosions which marked the beginning of the anomalous period. The vertical dashed line on 21 December marks the appearance of the shallowest VLP source (see Figure 4). This date separates the two time intervals used for deriving the correlation between VLP and gas time series.

5. Discussion

[37] In the following, we present our current state-of-the-art understanding of volcanic degassing at Etna in order to perform a direct comparison between the gas flux inferred from VLP event inversions and the observed gas fluxes. In order to deepen our understanding of the coupling between degassing and geophysical signals, we then examine a time series analysis of tremor, VLP events, and gas flux. We then conclude the discussion by asking the relationship between VLP events and gas flux investigation in the magma dynamics at Etna volcano.

5.1. Volcanic Degassing at Etna: The Relative Contribution of VLP Events to SO_2 Fluxes

[38] Our constraints on degassing fluxes at Mount Etna come from measurements of SO_2 flux. SO_2 is typically the third most abundant volatile component in volcanic plumes after H_2O and CO_2. *Shinohara et al*. [2008] and *La Spina et al*. [2010] reported quantitative measurements of the degassing flux of H_2O, CO_2, and SO_2 from individual craters of Mount Etna, revealing overall molar gas compositions, as shown in Table 1.

[39] SO_2 contributes 1–3 mol % of the total bulk gas plume emissions. There can be large differences in the gas composition emitted from each crater [*Burton et al*., 2005], suggesting a branched conduit geometry. The Northeast Crater (NEC) produces gas which is much poorer in CO_2 and richer in H_2O than that observed from the Central Crater (CC) [*Aiuppa et al*., 2008; *La Spina et al*., 2010]. *La Spina et al*. [2010] utilized a simple mass-conservation model to constrain the depth of a conduit branch at 60 MPa (~2.4 km assuming a lithospheric density controlled pressure gradient), well below that of the VLP source localization presented here, suggesting that the VLPs occur within either both branches or a single branch of the shallow conduit system.

[40] We wish to compare the amount of SO_2 involved in VLP events with the overall SO_2 flux, as this is the gas whose flux is measured at the surface. In order to do this, we need an estimate for the SO_2 mol % of gas at the VLP source depth of 1 km, with an estimated pressure of ~25 MPa. As discussed above, the SO_2 concentration is different for the two main branches of the conduit system, so we have two estimates at 25 MPa: 4 mol % for the NEC and 1 mol % for the CC, both derived from the models and assumptions presented in *La Spina et al*. [2010]. Assuming ideal gas behavior, the total number of moles N_m in 1 m^3 of gas at 25 MPa and 1423 K is calculated using PV/RT, where P is pressure in pascals, V is volume in cubic meters, R is the ideal gas constant (8.314 J^{-1} K mol^{-1}), and T is temperature in kelvins. This yields $N_m = (25 \times 10^6)/(8.314 \times 1423) = 2.1 \times 10^3$. Once accounting for uncertainties, the daily VLP volume changes inferred from the VLP events in section 4 have maximum and minimum values of 2.6×10^4 and 1.8×10^3 m^3, respectively (Figure 9). The number of moles associated with these events is therefore a maximum of $N_m \times 2.6 \times 10^4 = 5.5 \times 10^7$ mol and a minimum of $N_m \times 1.8 \times 10^3 = 3.8 \times 10^6$ mol. Using a weighted average volcanic gas molecular weight of 21 g, these molar quantities represent, for the maximum and minimum daily VLP volume changes, 1155 and 80 t/d of volcanic gas, respectively. Within the NEC with 4 mol % SO_2, the total SO_2 flux associated with VLP events would span between 10 and 140 t/d in the case that all VLP events occurred within the NEC conduit. Instead, within the CC with 1 mol % SO_2, the total SO_2 flux associated with VLP events would span between 2.5 and 35 t/d in the case that all VLP events occurred within the CC conduit. The average SO_2 fluxes from Etna in this period were 5300 t/d, and therefore, the maximum possible percentage of gas contribution arising from VLP activity is only 2.6% of the total observed SO_2 flux. However, if we consider a typical degassing period recorded on Etna, when fluxes are ~3000 t/d SO_2, this maximum possible percentage of gas associated with VLP events makes up less than 5% of the total degassing flux.

[41] These estimates of SO_2 gas amounts implicitly assume that the gas involved in each VLP event is in equilibrium with magma at the VLP source depth. This may not be the case; at Stromboli, the gas composition of explosions indicates the rapid ascent of gas from below the VLP source depth. Since the relative proportion of SO_2 decreases with increasing pressure, our estimates of the potential SO_2 content of the Etna VLPs should be therefore seen as upper limits; if the gas powering the VLP events was travelling from a deeper point in the feeding system, then they would be even poorer in SO_2.

Table 1. Molar Compositions of the Total Gas Flux Emitted From Mt. Etna, 2005–2009

Date	H_2O mol %	CO_2 mol %	SO_2 mol %	Reference
August 2005	82	15	3	*Shinohara et al*. [2008]
May 2006	81	18	1	*Shinohara et al*. [2008]
July 2007	86	11	3	*Shinohara et al*. [2008]
July 2008	82	16	2	*La Spina et al*. [2010]
August 2009	88	11	1	*La Spina et al*. [2010]

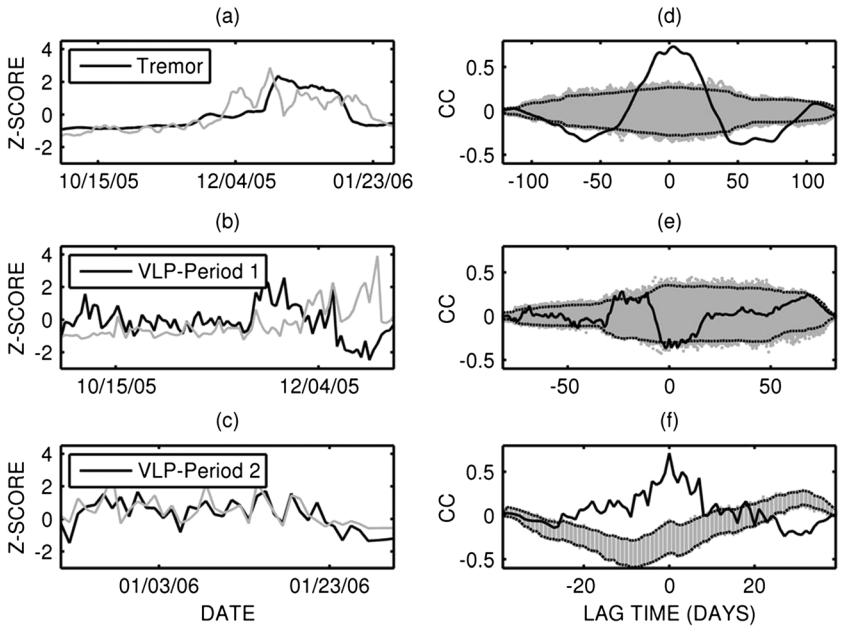

Figure 10. The SO_2 gas flux time series (gray line) compared with (a) RMS tremor amplitude and (b and c) VLP daily cumulative volume changes for Periods I and II, respectively. For obtaining these figures, each time series was first demeaned and then divided by the standard deviation (*z* score process). The tremor and gas flux data in Figure 10a were also smoothed with a 7 day long rectangular window in order to better highlight their similitude over long time spans. (d–f) The cross-correlation functions between the time series in Figures 10a–10c. Black lines are the cross correlations obtained over the original data; gray lines are the cross-correlation estimates derived by randomizing the SO_2 gas flux time series. Dotted black lines mark the 99% (±3σ) confidence bounds on the distribution of the correlation values obtained at individual time lags [see equation 5]. Periods I and II refer to the [01 October 2005 to 21 December 2005] and [22 December 2005 to 31 January 2006] time intervals, respectively.

[42] Using the magnitude of gas amount involved in a VLP event, we may assess to what degree they may be detectable as an increase in gas emission rate at the surface over and above the persistent degassing. Clearly, the intensity, and therefore detectability, of a gas release of a certain mass will depend on the time scale over which the gas mass is emitted and the variability of the background degassing. Here we calculate the longest time scale for the VLP gas release that would render it detectable at the surface using a SO_2 camera [e.g., *Mori and Burton*, 2006, 2009], which allows up to 1 Hz frequency SO_2 flux measurements. The typical background SO_2 gas flux is ~12 kg s^{-1} for the NEC and ~17 kg s^{-1} for the CC. Assuming natural variability of a factor of 2 in the background degassing SO_2 flux, the detection limit for VLP degassing becomes ~23 kg s^{-1} for the NEC and ~35 kg s^{-1} for the CC. These detection limits allow us to constrain the time scale over which the gas involved with a VLP event would have to be released in order for it to be detectable at the surface. In the case of the NEC, the slightly lower quiescent SO_2 flux and the relatively higher SO_2 content should make the VLP events easier to detect. Considering the frequency of VLP events per day (Figure 5a), the gas release time scale should range between 4 and 60 s for the VLP pulses to be detectable. On the other hand, the larger total SO_2 flux and the lower SO_2 content of the VLP events at the CC makes them harder to detect. Indeed, they need to be released over a time scale between 1 and 10 s in order to be detected.

[43] High-frequency investigation of the gas release from each crater is required in order to detect, or not, the presence of excess gas release associated with VLP events.

5.2. Time Series Correlation Between Gas Flux, VLPs, and Tremor

[44] In section 4, we used the volumetric changes at the VLP source to constrain the amount of volatiles implied in the VLP-generating process. In addition to VLP events, seismic tremor activity may be also related to the degassing rate of the volcano [e.g., *Aiuppa et al*., 2010; *Patanè et al*., 2011].

[45] To examine the link between daily estimates of degassing rate, seismic tremor amplitude, and VLP volumetric changes, we now proceed to investigate the correlation between these time series. The most striking features arising from visual inspection of Figure 9 are as follows: (a) At long periods (>10–20 days), the time series of SO_2 flux and tremor amplitude exhibit a similar behavior, marked by a 1 monthlong increase starting on late November and a 1 monthlong decrease during the late portion of the investigated period; (b) the long-period components of VLP and SO_2 time series are significantly different; for instance, the largest amplitudes of gas flux are associated with a minimum of VLP volume changes, in correspondence of the two explosions (16 December) that marked the beginning of the "anomalous" period; and (c) this trend appears to change a few days after the December explosions, contemporaneously with the activation of the shallower VLP source (Figure 4 and

dashed line in Figure 9a). Since then, daily VLP volume changes exhibit a bell-shaped trend similar to that displayed by the SO_2 time series. These two time spans correspond respectively to the first 82 days (1 October to 21 December) and the last 40 days (22 December 2005 to 1 February 2006) of observations. Throughout the following, we refer to these two intervals as Periods I and II, respectively.

[46] Following these arguments, we calculated the cross-correlation function between (1) tremor and SO_2 fluxes, after smoothing both time series using a 7 day long rectangular window, and (2) raw VLP volumes and SO_2 fluxes for both Periods I and II. Before proceeding with cross-correlation estimates, the three time series are standardized through demeaning and division by the respective standard deviations (Figure 10, left column). Our correlation estimates are based on a total of 123 values for each time series (4 months of data). Therefore, the correlation coefficients could not be very significant as a consequence of the low number of points. In order to test the statistical significance of the retrieved cross-correlation functions, we repeated the analysis a large number (10,000) of times, randomizing at each run the SO_2 time series. This is the same procedure used by *Martini et al*. [2009] to correlate the rainfall and seismicity at Fogo volcano (Sao Miguel, Azores). Results from this procedure are shown in Figure 10 (right column).

[47] To evaluate the mean and standard deviation of these "randomized correlations," we must consider that the correlation coefficients, being a normalized quantity, do not follow a Gaussian distribution. To compensate for this, we use Fisher's z transform to transform the calculated correlation coefficients into z, a new variable following a Gaussian distribution [e.g., *Saccorotti and Del Pezzo*, 2000], and we obtain average correlation coefficients and a relative standard deviation, i.e.,

$$z = \frac{1}{2}\ln\left(\frac{1+c}{1-c}\right) \tag{3}$$

[48] From the arithmetic mean and standard deviation of z, we can thus obtain an unbiased estimate of the first-moment statistics of coefficients c using the generic inverse transform

$$\hat{c} = \tanh(\bar{z}) \tag{4}$$

and relative standard deviation

$$\sigma c = \tanh(\sigma z) \tag{5}$$

[49] For each lag time of the randomized cross-correlation functions, we could thus establish the 99% ($\pm 3\sigma$) confidence bounds for assessing the significance of the cross correlations calculated using the original time series.

[50] Low-pass-filtered tremor amplitudes and SO_2 fluxes are linearly related (Figure 10): the respective cross correlation has a maximum value of about 0.74, which is well above the 99% significance level described above. This peak value is associated with a lag time of 3 days, corresponding to a delay of the tremor time series with respect to the gas one. Due to the broadness of the correlation peak, however, we do not deem that lag time is particularly significant.

[51] During Period I, the time series of VLP volumes and SO_2 fluxes are poorly related. With the exception of a few points, the cross-correlation function never passes the 99% significance test. Conversely, the VLP volumes and SO_2 fluxes for Period II exhibit a significant (0.72), zero-lag correlation, indicating the coupling between the two processes.

5.3. Source Process for Volcanic Tremor, VLP Events, and SO_2 Flux

[52] The empirical observation of correlations between the long-period components of volcanic tremor and SO_2 flux during a period of quiescence at Mount Etna suggests a common causal process which links the two phenomena. *Burton et al*. [2007] showed that for Stromboli magmas, which have a similar original volatile content as those for Etna, closed-system degassing occurs during ascent until a pressure of 50–75 MPa, when the system becomes sufficiently vesicular to permit permeable fluid flow. Such a flow of gas through the magma column may produce volcanic tremor signals, as permeable channels open and close, modulating pressure and gas transport rate. In such a scenario, a strong correlation between volcanic tremor and gas flux, such as that observed on Etna during the period of study, is expected.

[53] It is more difficult to interpret the time- and space-dependent correlations exhibited by VLP source volumes and SO_2 flux time series. VLP sources are commonly interpreted in terms of pressure pulses resulting from transient instabilities in magma-gas two-phase flows [e.g., *Chouet*, 2003]. In particular, gas slugs undergoing an abrupt flow pattern change upon entering a section of a significantly increased conduit diameter may be a source for such instabilities [e.g., *James et al*., 2006]. As for the establishment of a well-developed, intermittent slug-flow regime, different models exist for which bubble coalescence and slug formation are mostly controlled by either flow velocities [e.g., *Parfitt*, 2004, and references therein] or geometrical complexities of the plumbing system [e.g., *Jaupart and Vergniolle*, 1988; *James et al*., 2006]. With the data presently available, it is impossible to distinguish which of these different, competing models is the most appropriate model for interpreting our observations. In general, we can only state that the amount of volatiles involved into the VLP-generating process scales linearly with the SO_2 released at the surface only under particular circumstances. According to our analysis, these conditions could be related to the particular location of the source (and, hence, to the geometry of the conduit), to the absolute gas emission rates, or both.

6. Conclusions

[54] We have applied an inversion procedure to seismic measurements of very long period (VLP) events in order to determine the volume change associated with the events. Interpreting the results of these inversions in light of SO_2 flux degassing measurements reveals the following main points. The VLP rate on Etna shows large variability and appears to vary as a function of volcanic activity. The gas associated with VLPs makes up, at most, 5% of the total degassing flux, but if the gas associated with these events is released sufficiently swiftly (over between 10 and 60 s depending on the crater), then the VLP gas loss may be measurable with a SO_2 camera.

[55] Throughout the analyzed time interval, the correlation between VLP volume changes and SO_2 fluxes establishes only for a particular location of the VLP source. Even if limited in time, such correlation suggests that VLP signals are causally related to magma degassing. The dependence of

such coupling on the spatial location of the seismic source suggests that the geometry of the plumbing system plays a major role in controlling flow instabilities sourcing VLP pulses. Further observational data and analogue experiments of the two-phase flow in geometrically complex conduit systems are, however, needed in order to better elucidate the significance of the above observations.

[56] On the other side, the long-term correlation exhibited by tremor and SO_2 fluxes suggests that the former parameter is likely associated with the persistent flux of gases throughout a permeable network of interconnected vesicles developing within the uppermost portion of the volcano's plumbing system.

[57] Such linear relationship opens interesting perspective toward utilization of tremor signal as a proxy for evaluating the long-term degassing activity of a volcano.

[58] **Acknowledgments.** We would like to thank I. Lokmer, L. De Barros, D. Carbone, F. Martini, and A. Brancato for useful comments on the manuscript. The paper benefited from thoughtful revisions by Philippe Lesage and an anonymous reviewer.

References

Aiuppa, A., S. Bellomo, W. D'Alessandro, C. Federico, M. Ferm, and M. Valenza (2004), Volcanic plume monitoring at Mount Etna by diffusive (passive) sampling, *J. Geophys. Res.*, *109*, D21308, doi:10.1029/2003JD004481.

Aiuppa, A., G. Giudice, S. Gurrieri, M. Liuzzo, M. Burton, T. Caltabiano, A. J. S. McGonigle, G. Salerno, H. Shinohara, and M. Valenza (2008), Total volatile flux from Mount Etna, *Geophys. Res. Lett.*, *35*, L24302, doi:10.1029/2008GL035871.

Aiuppa, A., et al. (2010), Patterns in the recent 2007–2008 activity of Mount Etna volcano investigated by integrated geophysical and geochemical observations, *Geochem. Geophys. Geosyst.*, *11*, Q09008, doi:10.1029/2010GC003168.

Allard, P., P. Jean-Baptiste, W. D'Alessandro, F. Parello, B. Parisi, and C. Flehoc (1997), Mantle-derived helium and carbon in groundwaters and gases of Mount Etna, Italy, *Earth Planet. Sci. Lett.*, *148*, 501–516.

Alparone, S., D. Andronico, L. Lodato, and T. Sgroi (2003), Relationship between tremor and volcanic activity during the southeast crater eruption on Mount Etna in early 2000, *J. Geophys. Res.*, *108*(B5), 2241, doi:10.1029/2002JB001866.

Alparone, S., B. Behncke, S. Giammanco, M. Neri, and E. Privitera (2005), Paroxysmal summit activity at Mt. Etna (Italy) monitored through continuous soil radon measurements, *Geophys. Res. Lett.*, *32*, L16307, doi:10.1029/2005GL023352.

Andronico, D., et al. (2005), A multidisciplinary study of the 2002–03 Etna eruption: Insights into a complex plumbing system, *Bull. Volcanol.*, *67*, 314–330, doi:10.1007/s00445-004-0372-8.

Arciniega-Ceballos, A., C. Valdes-Gonzalez, and P. Dawson (2000), Temporal and spectral characteristics of seismicity observed at Popocatepetl volcano, central Mexico, *J. Volcanol. Geotherm. Res.*, *102*, 207–216.

Arciniega-Ceballos, A., B. Chouet, P. Dawson, and G. Asch (2008), Broadband seismic measurements of degassing activity associated with lava effusion at Popocatépetl Volcano, Mexico, *J. Volcanol. Geotherm. Res.*, *170*, 12–23.

Aster, R., D. Zandomeneghi, S. Mah, S. McNamara, D. B. Henderson, H. Knox, and K. Jones (2008), Moment tensor inversion of very long period seismic signals from Strombolian eruptions of Erebus volcano, *J. Volcanol. Geotherm. Res.*, *177*, 635–647, doi:10.1016/j.jvolgeores.2008.08.013.

Behncke, B., M. Neri, E. Pecora, and V. Zanon (2006), The exceptional activity and growth of the southeast Crater, Mt. Etna (Italy) between 1996 and 2001, *Bull. Volcanol.*, *69*, 149–173.

Burton, M. R., et al. (2005), Etna 2004–2005: An archetype for geodynamically-controlled effusive eruptions, *Geophys. Res. Lett.*, *32*, L09303, doi:10.1029/2005GL022527.

Burton, M. R., H. M. Mader, and M. Polacci (2007), The role of gas percolation in quiescent degassing of persistently active basaltic volcanoes, *Earth Planet. Sci. Lett.*, *264*, 46–60, doi:10.1016/j.epsl.2007.08.028.

Caltabiano, T., M. Burton, S. Giammanco, P. Allard, N. Bruno, F. Murè, and R. Romano (2004), Volcanic gas emissions from the summit craters and flanks of Mt. Etna, 1987–2000, in *Mt. Etna: Volcano Laboratory*, Geophys. Monogr. Ser., vol. *143*, edited by A. Bonaccorso et al., pp. 111–128, AGU, Washington, D. C.

Cannata, A., M. Hellweg, G. Di Grazia, S. Ford, S. Alparone, S. Gresta, P. Montalto, and D. Patanè (2009), Long period and very long period events at Mt. Etna volcano: Characteristics, variability and causality, and implications for their sources, *J. Volcanol. Geotherm. Res.*, *187*, 227–249, doi:10.1016/j.jvolgeores.2009.09.007.

Carbone, D., L. Zuccarello, G. Saccorotti, and F. Greco (2006), Analysis of simultaneous gravity and tremor anomalies observed during the 2002–2003 Etna eruption, *Earth Planet. Sci. Lett.*, *245*, 616–629.

Carbone, D., L. Zuccarello, and G. Saccorotti (2008), Geophysical indications of magma uprising at Mt. Etna during the December 2005 to January 2006 non-eruptive period, *Geophys. Res. Lett.*, *35*, L06305, doi:10.1029/2008GL033212.

Chouet, B. (2003), Volcano seismology, *Pure Appl. Geophys.*, *160*, 739–788.

Chouet, B., P. Dawson, T. Ohminato, M. Martini, G. Saccorotti, F. Giudicepietro, G. De Luca, G. Milana, and R. Scarpa (2003), Source mechanism of explosions at Stromboli Volcano, Italy, determined from moment-tensor inversions of very-long-period data, *J. Geophys. Res.*, *108*(B1), 2019, doi:10.1029/20042JB001919.

Chouet, B., P. Dawson, and A. Arciniega-Ceballos (2005), Source mechanism of Vulcanian degassing at Popocatépetl volcano, Mexico, determined from waveform inversions of very long period signals, *J. Geophys. Res.*, *110*, B07301, doi:10.1029/2004JB003524.

Chouet, B., P. Dawson, and M. Martini (2008), Shallow-conduit dynamics at Stromboli Volcano, Italy, imaged from waveform inversions, *Geol. Soc. Spec. Publ.*, *307*, 57–84, doi:10.1144/SP307.5.

Chouet, B., P. Dawson, M. R. James, and S. J. Lane (2010), Seismic source mechanism of degassing bursts at Kilauea Volcano, Hawaii: Results from waveform inversion in the 10–50 s band, *J. Geophys. Res.*, *115*, B09311, doi:10.1029/2009JB006661.

De Barros, L., C. J. Bean, I. Lokmer, G. Saccorotti, L. Zuccarello, G. S. O'Brien, G. J. Métaxian, and D. Patanè (2009), Source geometry from exceptionally high resolution long period event observations at Mt. Etna during the 2008 eruption, *Geophys. Res. Lett.*, *36*, L24305, doi:10.1029/2009GL041273.

De Barros, L., I. Lokmer, C. J. Bean, G. S. O'Brien, G. Saccorotti, G. J. Métaxian, L. Zuccarello, and D. Patanè (2011), Source mechanism of long period events recorded by a high density seismic network during the 2008 eruption on Mount Etna, *J. Geophys. Res.*, *116*, B01304, doi:10.1029/2010JB007629.

De Guidi, G., S. Scudero, and S. Gresta (2012), New insights into the local crust structure of Mt. Etna volcano from seismological and morphotectonic data, *J. Volcanol. Geotherm. Res.*, *223–224*, 83–92, doi:10.1016/j.jvolgeores.2012.02.001.

Di Grazia, G., S. Falsaperla, and H. Langer (2006), Volcanic tremor location during the 2004 Mount Etna Lava effusion, *Geophys. Res. Lett.*, *33*, L04304, doi:10.1029/2005GL025177.

Di Grazia, G., A. Cannata, P. Montalto, D. Patanè, E. Privitera, L. Zuccarello, and E. Boschi (2009), A new approach to volcano monitoring based on 4D analyses of seismo-volcanic and acoustic signals: The 2008 Mt. Etna eruption, *Geophys. Res. Lett.*, *36*, L18307, doi:10.1029/2009GL039567.

James, M. R., S. J. Lane, B. Chouet, and J. S. Gilbert (2004), Pressure changes associated with the ascent and bursting of gas slugs in liquid-filled vertical and inclined conduits, *J. Volcanol. Geotherm. Res.*, *129*, 61–82.

James, M. R., S. J. Lane, and B. A. Chouet (2006), Gas slug ascent through changes in conduit diameter: Laboratory insights into a volcano-seismic source process in low-viscosity magmas, *J. Geophys. Res.*, *111*, B05201, doi:10.1029/2005JB003718.

Jaupart, C., and S. Vergniolle (1988), Laboratory models of Hawaiian and Strombolian eruptions, *Nature*, *331*, doi:10.1038/331058a0.

Kanasewich, E. R. (1981), *Time sequence Analysis in Geophysics*, Univ. of Alberta Press, Edmonton, Alberta, Canada, pp. 1–532.

Kawakatsu, H., S. Kaneshima, H. Matsubayashi, T. Ohminato, Y. Sudo, T. Tsutsui, K. Uhira, H. Yamasato, H. Ito, and D. Legrand (2000), Aso94: Aso seismic observation with broadband instruments, *J. Volcanol. Geotherm. Res.*, *101*, 129–154.

Kazahaya, R., T. Mori, M. Takeo, T. Ohminato, T. Urabe, and Y. Maeda (2011), Relation between single very-long-period pulses and volcanic gas emissions at Mt. Asama, Japan, *Geophys. Res. Lett.*, *38*, L11307, doi:10.1029/2011GL047555.

La Spina, A., M. Burton, and G. G. Salerno (2010), Unravelling the processes controlling gas emissions from the central and northeast craters of Mt. Etna, *J. Volcanol. Geotherm. Res.*, *198*, 368–376, doi:10.1016/j.jvolgeores.2010.09.018.

Lokmer, I., C. J. Bean, G. Saccorotti, and D. Patanè (2007), Moment-tensor inversion of LP events recorded on Etna in 2004 using constraints obtained from wave simulation tests, *Geophys. Res. Lett.*, *34*, L22316, doi:10.1029/2007GL031902.

Lyons, J. J., and G. P. Waite (2011), Dynamics of explosive volcanism at Fuego volcano imaged with very long period seismicity, *J. Geophys. Res.*, *116*, B09303, doi:10.1029/2011JB008521.

Marchetti, E., and M. Ripepe (2005), Stability of the seismic source during effusive and explosive activity at Stromboli Volcano, *Geophys. Res. Lett.*, *32*, L03307, doi:10.1029/2004GL021406.

Martini, F., C. J. Bean, G. Saccorotti, F. Viveiros, and N. Wallenstein (2009), Seasonal cycles of seismic velocity variations detected using coda wave interferometry at Fogo volcano, São Miguel, Azores, during 2003–2004, *J. Volcanol. Geotherm. Res.*, *181*, 231–246.

Matsubara, W., and M. Yomogida (2004), Source process of low-frequency earthquakes associated with the 2000 eruption of Mt. Usu, *J. Volcanol. Geotherm. Res.*, *134*, 223–240.

Mori, T., and M. Burton (2006), The SO_2 camera: A simple, fast and cheap method for groundbased imaging of SO_2 in volcanic plumes, *Geophys. Res. Lett.*, *33*, L24804, doi:10.1029/2006GL027916.

Mori, T., and M. Burton (2009), Quantification of the gas mass emitted during single explosions on Stromboli with the SO_2 imaging camera, *J. Volcanol. Geotherm. Res.*, *188*, 395–400, doi:10.1016/j.jvolgeores.2009.10.005.

Muller, G. (2001), Volume change of seismic sources from moment tensors, *Bull. Seismol. Soc. Am.*, *91*, 880–884.

Nadeau, P. A., J. L. Palma, and G. P. Waite (2011), Linking volcanic tremor, degassing, and eruption dynamics via SO_2 imaging, *Geophys. Res. Lett.*, *38*, L01304, doi:10.1029/2010GL045820.

Neidell, N., and M. T. Taner (1971), Semblance and other coherency measures for multichannel data, *Geophysics*, *36*, 482–497.

Neri, M., B. Behncke, M. Burton, G. Galli, S. Giammanco, E. Pecora, E. Privitera, and D. Reitano (2006), Continuous soil radon monitoring during the July 2006 Etna eruption, *Geophys. Res. Lett.*, *33*, L24316, doi:10.1029/2006GL028394.

Neuberg, J., and T. Pointer (2000), Effects of volcano topography on seismic broad-band waveforms, *Geophys. J. Int.*, *143*, 239–248.

O'Brien, G. S., and C. J. Bean (2008), Seismicity on volcanoes generated by gas slug ascent, *Geophys. Res. Lett.*, *35*, L16308, doi:10.1029/2008GL035001.

Ohminato, T. (2006), Characteristics and source modeling of broadband seismic signals associated with the hydrothermal system at Satsuma-IwoJima volcano, Japan, *J. Volcanol. Geotherm. Res.*, *158*, 467–490.

Oppenheimer, C., B. Scaillet, and R. S. Martin (2011), Sulfur degassing from volcanoes: Source conditions, surveillance, plume chemistry and earth system impacts, *Rev. Mineral. Geochem.*, *73*(1), 363–421, doi:10.2138/rmg.2011.73.13.

Parfitt, E. (2004), A discussion of the mechanisms of explosive basaltic eruptions, *J. Volcanol. Geotherm. Res.*, *134*, 77–107.

Patanè, D., G. Di Grazia, C. Cannata, P. Montalto, and E. Boschi (2008), Shallow magma pathway geometry at Mt. Etna Volcano, *Geochem. Geophys. Geosyst.*, *9*, Q12021, doi:10.1029/2008GC002131.

Patanè, D., M. Aliotta, A. Cannata, C. Cassisi, M. Coltelli, G. Di Grazia, P. Montalto, and L. Zuccarello (2011), Interplay between tectonics and Mount Etna's volcanism: Insights into the geometry of the plumbing system, in *New Frontiers in Tectonic Research—At the Midst of Plate Convergence*, edited by U. Schattner, pp. 73–104, InTech, Croatia.

Patanè, D., et al. (2013), Insights into magma and fluid transfer at Mount Etna by a multiparametric approach: A model of the events leading to the 2011 eruptive cycle, *J. Geophys. Res. Solid Earth*, *118*, 3519–3539, doi:10.1002/jgrb.50248.

Rowe, C. A., R. C. Aster, P. R. Kyle, J. W. Schlue, and R. R. Dibble (1998), Broadband recording of Strombolian explosions and associated very-long-period seismic signals on Mount Erebus Volcano, Ross Island, Antarctica, *Geophys. Res. Lett.*, *25*, 2297–2300, doi:10.1029/98GL01622.

Saccorotti, G., and E. Del Pezzo (2000), A probabilistic approach to the inversion of data from a seismic array and its application to volcanic signals, *Geophys. J. Int.*, *143*, 249–261.

Saccorotti, G., I. Lokmer, C. J. Bean, G. Di Grazia, and D. Patanè (2007), Analysis of sustained long-period activity at Etna volcano, Italy, *J. Volcanol. Geotherm. Res.*, *160*, 340–354.

Salerno, G. G., M. R. Burton, C. Oppenheimer, T. Caltabiano, V. I. Tsanev, and N. Bruno (2009a), Novel retrieval of volcanic SO2 abundance from ultraviolet spectra, *J. Volcanol. Geotherm. Res.*, *181*, 141–153, doi:10.1016/j.jvolgeores.2009.01.009.

Salerno, G. G., M. R. Burton, C. Oppenheimer, T. Caltabiano, D. Randazzo, N. Bruno, and V. Longo (2009b), Three-years of SO_2 flux measurements of Mt. Etna using an automated UV scanner array: Comparison with conventional traverses and uncertainties in flux retrieval, *J. Volcanol. Geotherm. Res.*, *183*, 76–83, doi:10.1016/j.jvolgeores.2009.02.013.

Shinohara, H., A. Aiuppa, G. Giudice, S. Gurrieri, and M. Liuzzo (2008), Variation of H_2O/CO_2 and CO_2/SO_2 ratios of volcanic gases discharged by continuous degassing of Mount Etna volcano, Italy, *J. Geophys. Res.*, *113*, B09203, doi:10.1029/2007JB005185.

Vergniolle, S., and Y. Gaudemer (2011), Decadal evolution of a degassing magma reservoir unravelled from fire fountains produced at Etna volcano (Italy) between 1989 and 2001, *Bull. Volcanol.*, doi:10.1007/s00445-011-0563-z.